Journal of Materials Chemistry A

PAPER

View Article Online
View Journal | View Issue

Cite this: J. Mater. Chem. A, 2019, 7, 7760

Employing structurally similar acceptors as crystalline modulators to construct high efficiency ternary organic solar cells†

Huanxiang Jiang,‡[ad] Xiaoming Li,‡[a] Zezhou Liang,[a] Gongyue Huang,[a] Weichao Chen,*[b] Nan Zheng*[c] and Renqiang Yang*[a]

Received 28th December 2018
Accepted 28th February 2019

DOI: 10.1039/c8ta12481g

rsc.li/materials-a

Two structurally similar acceptors ITIC and IT-4F with complementary absorption spectra were employed to construct high-performance ternary blend polymer solar cells (PSCs) by combining a new polymer donor PBTA-PS. The ternary blend solar cell exhibits an outstanding power conversion efficiency of 13.27% with an enhanced short circuit current density (J_{SC}) of 19.60 mA cm^{-2} and an excellent fill factor of 74.45%, which is higher than that of PBTA-PS:ITIC (IT-4F) binary solar cells. A wide photoresponse resulting in large J_{SC}, and good miscibility and compatibility of the three components guarantee the desired morphology and molecular packing in the ternary blend film, which improved the charge transport properties. Our results demonstrated that employing structurally similar acceptors is a promising strategy to enhance the molecular packing and realize high-performance ternary solar cells.

Introduction

Polymer solar cells (PSCs) have attracted tremendous attention around the world on account of their solution processability, 珠exibility and light weight, which make them a potential technology to utilize the solar energy. The past decade has witnessed the rapid progress of the power conversion efficiency (PCE) of PSCs.[1–9] To date, the PCEs of single junction bulk-heterojunction (BHJ) PSCs have exceeded 14% by designing novel conjugated polymers and non-fullerene acceptors (NFAs) as well as interface engineering.[10–16] Moreover, the development of device structures and processing methods also promotes the performance of PSCs. However, the narrow absorption band of organic semiconductor materials makes it hard to harvest photons in a wide range.[17–20] Therefore, it's essential to enhance the light harvesting ability of PSCs by employing multiple donors and acceptors with complementary absorption and thereby improve the photocurrent.

One strategy is combining three photovoltaic materials (two donors with one acceptor or one donor with two acceptors) with complementary absorption to fabricate single junction solar cells, known as ternary solar cells. This method could broaden the absorption range of the PSCs while retaining the simple fabricating process of single junction devices.[21–29] As for ternary solar cells, a bicontinuous interpenetrating network is required for efficient exciton dissociation and charge transport. As a consequence, the morphology of active layers is of vital importance. In many cases, the incorporation of a third component in the active layer will disturb the phase separation and molecular orientation of the binary blend. Particularly in ternary systems containing two donor polymers, the poor miscibility of polymers remains an obstacle in achieving the ideal morphology. Therefore, with the rapid development of NFAs, more and more research efforts have been devoted to ternary systems based on two acceptors, either one fullerene derivative combined with one NFA or two NFAs. A PCE of over 13% has been obtained for ternary systems based on one fullerene derivative and one NFA.[30,31] As for the ternary system based on two NFAs, many studies have also been carried out. For instance, Sun and co-workers 珡rst fabricated a ternary PSC based on two NFAs (SdiPBI-Se and ITIC-Th) with a high PCE exceeding 10%.[32,33] Hou and co-workers fabricated a ternary PSC using IT-M and IEICO as acceptors, which delivered a high PCE of 11.1%. Chen and co-workers used NNBDT and FDNCTF as acceptors to fabricate a ternary PSC which exhibited high performance with a PCE of 12.8%.[34] Zhang and co-workers fabricated a high performance ternary PSC with a PCE of 13.7% utilizing INPIC and MeICl as acceptors.[35] As a consequence, these results guarantee a promising future for non-fullerene ternary PSCs.[36–38]

[a]CAS Key Laboratory of Bio-based Materials, Qingdao Institute of Bioenergy and Bioprocess Technology, Chinese Academy of Sciences, Qingdao 266101, China. E-mail: yangrq@qibebt.ac.cn

[b]College of Textiles & Clothing, State Key Laboratory of Bio-珡bers and Eco-textiles, Collaborative Innovation Center for Eco-Textiles of Shandong Province, Qingdao University, Qingdao 266071, China. E-mail: chenwc@qdu.edu.cn

[c]Institute of Polymer Optoelectronic Materials and Devices, State Key Laboratory of Luminescent Materials and Devices, South China University of Technology, Guangzhou 510640, China. E-mail: zhengn@scut.edu.cn

[d]University of Chinese Academy of Sciences, Beijing 100049, China

† Electronic supplementary information (ESI) available. See DOI: 10.1039/c8ta12481g

‡ Huanxiang Jiang and Xiaoming Li contributed equally to this work.

In this contribution, high efficiency ternary blend PSCs were fabricated by combining a new medium bandgap polymer PBTA-PS and two structurally similar NFAs (ITIC and IT-4F). The binary devices based on the polymer deliver PCEs of 11.83% and 9.55% for ITIC and IT-4F as acceptors, respectively. The PBTA-PS:ITIC binary device showed higher open circuit voltage (V_{OC}) and 珡ll factor (FF), but lower short circuit current density (J_{SC}) than the PBTA-PS:IT-4F device. A泖er adding a small amount of IT-4F into the PBTA-PS:ITIC system, the J_{SC} and FF increased simultaneously, while the V_{OC} decreased slightly. Hence, the ternary PSC displayed a high PCE of 13.27% with a J_{SC} of 19.60 mA cm^{-2}, a relatively high V_{OC} of 0.91 V and a superior FF of 74.45%. The enhanced J_{SC} and FF could be attributed to the complementary absorption and improved crystallinity because of the similar chemical structure between ITIC and IT-4F, endowing them with good miscibility and compatibility in the ternary blend. As a consequence, IT-4F could act as a crystalline modulator to enhance the molecular packing. In addition, efficient energy transfer was observed from ITIC to IT-4F, which could promote the exciton dissociation efficiency. Our results demonstrated that choosing structurally similar acceptors is a promising approach to enhance the crystallinity of polymers and enable efficient energy transfer synergistically for realizing high-efficiency ternary PSCs.

Result and discussion

The chemical structures of PBTA-PS, ITIC and IT-4F are shown in Fig. 1a. The synthesis procedure and characterization of PBTA-PS are depicted in the ESI.† The polymer PBTA-PS was obtained through Stille polymerization using $Pd_2(dba)_3$ and P(*o*-tol)$_3$ as catalysts. The polymer could be dissolved in chloroform (CF), chlorobenzene (CB) and *o*-dichlorobenzene (*o*-DCB). The thermal stability of the polymer was tested by thermogravimetric analysis (TGA). PBTA-PS has high thermal stability with an onset decomposition temperature (T_d) of 334 °C with 5% weight loss (Fig. S2†). Demonstrating the thermal stability of PBTA-PS is important for PSC fabrication. The two acceptors shared the same core IDTT, the only difference between them is that IT-4F has a 玾uorine substituted end group. This could guarantee good miscibility and compatibility. Fluorine atoms could help lower the highest occupied molecular orbital (HOMO) and lowest unoccupied molecular orbital (LUMO), and cause a little red-shi泖 in the absorption. Thus, the two acceptors exhibit complementary absorption, as shown in Fig. 1b. The energy level alignment of PBTA-PS, ITIC and IT-4F is depicted in Fig. 1d. The ternary system possesses a cascade energy level alignment. The HOMOs of PBTA-PS, ITIC and IT-4F are —5.34 eV, —5.50 eV, and 5.66 eV, respectively. The LUMOs of PBTA-PS, ITIC and IT-4F are —3.40 eV, —3.89 eV and —4.14 eV, respectively. The LUMO and HOMO offset between PBTA-PS and acceptors is sufficient for exciton dissociation and charge transport. As shown in Fig. 1c, the binary and ternary blend PSCs were fabricated with a conventional device structure of indium tin oxide (ITO) glass/poly(3,4-ethylenedioxythiopene):poly(styrenesulfonate) (PEDOT:PSS)/PBTA-PS:acceptors/perylene diimide functionalized with amino N-oxide (PDINO)/Al. The best weight ratio between PBTA-PS and ITIC is 1 : 1.2 (ESI†). Ternary PSCs were fabricated by varying the amount of IT-4F. PBTA-PS:ITIC and PBTA-PS:IT-4F binary PSCs were also fabricated for comparison. The device fabrication and optimization process are depicted in the ESI.†

The optimal current density–voltage (*J*–*V*) curves of binary PSCs are shown in Fig. 2a. The detailed photovoltaic parameters are listed in Table 1. The PBTA-PS:ITIC binary PSCs delivered a moderate PCE of 11.83% with a high V_{OC} of 0.95 V, a J_{SC} of 17.90 mA cm^{-2} and a 珡ll factor of 69.59%. The PBTA-PS:IT-4F PSCs exhibit an inferior PCE of 9.55% with a V_{OC} of 0.77 V, a J_{SC} of 18.31 mA cm^{-2} and a 珡ll factor of 67.62%. The large J_{SC} of PBTA-PS:IT-4F PSCs bene珡ts from the broad photoresponse of IT-4F. Therefore, IT-4F could be used as the third component to broaden the photoresponse range of PBTA-PS:ITIC binary PSCs for further improvement of PCE. Ternary PSCs were fabricated by introducing different amounts of IT-4F to the PBTA-PS:ITIC binary system. The weight ratio between PBTA-PS and ITIC was 珡xed at 1 : 1.2 (Fig. S4†). The corresponding photovoltaic parameters are listed in Table S2.† When the weight ratio of PBTA-PS : ITIC : IT-4F was 1 : 1.2 : 0.2, the ternary PSCs delivered a high PCE of 13.27% with a relatively high V_{OC} of 0.91 V, an enhanced J_{SC} of 19.60 mA cm^{-2} and a markedly improved FF of 74.45%. The corresponding *J*–*V* curve is shown in Fig. 2a. The enhanced PCE mainly bene珡ts from the simultaneously increased J_{SC} and FF, which could be

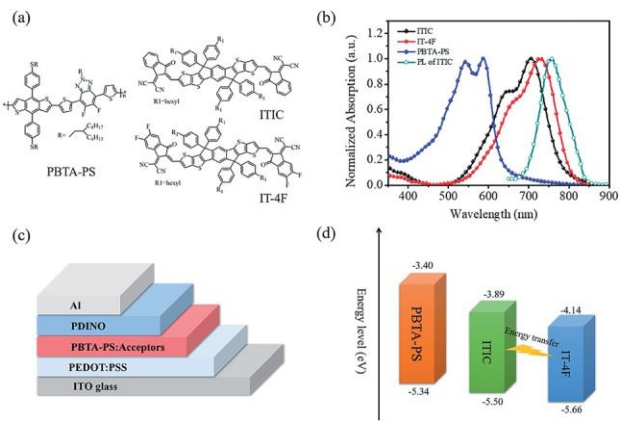

Fig. 1 (a) The chemical structures of PBTA-PS, ITIC and IT-4F. (b) The absorption spectra of PBTA-PS, ITIC, and IT-4F, and the photoluminescence (PL) spectrum of ITIC. (c) The diagram of a conventional device structure. (d) The energy level alignment of PBTA-PS, ITIC and IT-4F.

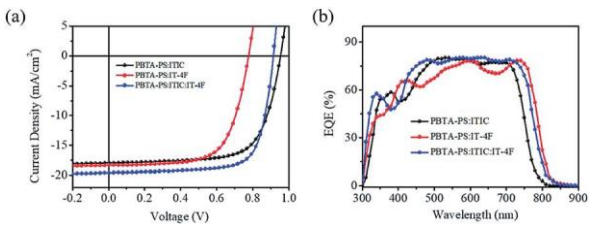

Fig. 2 (a) *J*–*V* curves of optimal binary and ternary devices. (b) EQE spectra of optimal binary and ternary devices.

Table 1 Photovoltaic parameters of optimal binary and ternary PSCs. The average efficiencies and standard deviations were calculated based on 20 cells prepared from different batches

Active layers	V_{OC} [V]	J_{SC} [mA cm^{-2}]	FF [%]	PCE [%]
PBTA-PS:ITIC	0.95 (0.95 ± 0.01)	17.90 (17.70 ± 0.23)	69.59 (68.87 ± 1.32)	11.83 (11.46 ± 0.39)
PBTA-PS:IT-4F	0.77 (0.77 ± 0.01)	18.31 (17.92 ± 0.52)	67.62 (65.48 ± 3.67)	9.55 (9.23 ± 0.25)
Ternary blend	0.91 (0.91 ± 0.01)	19.60 (19.28 ± 0.37)	74.45 (73.20 ± 1.54)	13.27 (13.09 ± 0.19)

attributed to the superior light harvesting and optimized charge transport. It is worth noting that the V_{OC} of ternary PSCs was not pinned at the smaller V_{OC} of the binary PSCs, it varies along with the change of the content of IT-4F. As the content of IT-4F increases, the V_{OC} decreases. A similar variation trend of V_{OC} was observed in some other ternary PSC studies, which could be well explained by the alloy model.[39,40]

To further investigate the photoresponse of PSCs, external quantum efficiencies (EQEs) were calculated. As shown in Fig. 2b the ternary PSC exhibits a wider photo-response range than the PBTA-PS:ITIC device due to the introduction of IT-4F. Meanwhile, high EQE values were achieved for the ternary devices with the maximum EQE approaching 80%. This indicates that the introduction of IT-4F did not disrupt the exciton dissociation process but realizes a broad photoresponse range. The J_{SC} values of PBTA-PS:ITIC, PBTA-PS:IT-4F and ternary PSCs calculated from the EQE spectra are 17.67, 18.60 and 19.28 mA cm^{-2}, respectively, which are consistent with the measured J_{SC}s with little error (<5%).

The exciton dissociation and charge collection processes in binary and ternary devices are further investigated by plotting the photocurrent (J_{ph} ¼ J_L — J_D) *versus* the effective applied voltage (V_{eff} ¼ V_0 — V), where J_L and J_D represent the current density under AM 1.5G illumination and in the dark state, respectively. V_0 is the voltage when J_L ¼ J_D. V is the applied voltage on the devices. As shown in Fig. 3a, when V_{eff} exceeds 1 V, the J_{ph} values of binary and ternary devices tend to reach the saturation value (J_{sat}), indicating little charge recombination at high bias voltage. The ratio of J_{ph}/J_{sat} under short circuit conditions can be calculated to estimate the overall charge dissociation probability.[41] The J_{sat} values of PBTA-PS:ITIC, PBTA-PS:IT-4F and ternary devices are 18.46 mA cm^{-2}, 19.29 mA cm^{-2} and 20.20 mA cm^{-2}, respectively. Correspondingly, the J_{ph}/J_{sat} values of PBTA-PS:ITIC, PBTA-PS:IT-4F and ternary devices are 96%, 94% and 97%, respectively. The ternary PSCs exhibit higher J_{sat} and J_{ph}/J_{sat}, illustrating that incorporation of IT-4F into PBTA-PS:ITIC could facilitate the exciton generation as well as the exciton dissociation process, resulting in more charges being collected by electrodes with little recombination. For more insight into the recombination behavior in the binary and ternary PSCs, the photocurrent J_{ph} as a function of light intensity (P_{light}) was plotted. The relationship between J_{ph} and P_{light} can be described with the power-law J_{SC} ∝ P^{α}, where α approaching 1 indicates negligible recombination.[42] As shown in Fig. 3b, the α of ternary PSCs is 0.99, which is slightly higher than that of the binary PSCs, manifesting that adding small amounts of IT-4F into the PBTA-PS:ITIC system could effectively suppress charge recombination, supporting the high J_{SC} and FF of ternary PSCs.

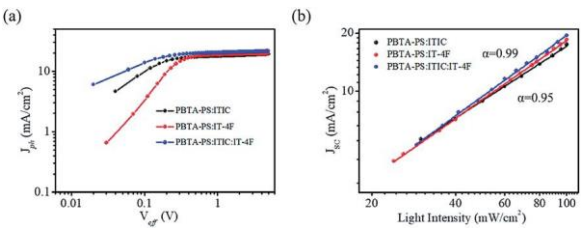

Fig. 3 The plots of (a) J_{ph} *versus* V_{eff} and (b) short circuit current density *versus* light intensity.

To further investigate the charge transport properties of binary and ternary PSCs, the electron and hole mobility was characterized by the space-charge-limited-current (SCLC) method.[43] Electron-only and hole-only diodes were fabricated using the con珐guration of ITO glass/ZnO/active layer/PDINO/Al and ITO glass/PEDOT:PSS/active layer/Au, respectively. The corresponding J–V curves are shown in Fig. S5.† The electron mobility (μ_e) and hole mobility (μ_h) values are listed in Table 2. The electron and hole mobilities of PBTA-PS:ITIC are 1.85 cm^2 V^{-1} s^{-1} and 2.86 × 10^{-4} cm^2 V^{-1} s^{-1}, respectively, which are slightly higher than those of the PBTA-PS:IT-4F counterpart. A沢er incorporating 20% (wt%) IT-4F into the PBTA-PS:ITIC system, the ternary system exhibits simultaneously increased electron and hole mobilities. The μ_e/μ_h became closer to 1, indicating a more balanced charge transport. Moreover, the balanced charge transport could effectively suppress the recombination and space-charge effect, leading to an excellent FF up to 74.45%.[44,45]

Photoluminescence (PL) studies were performed to gain insight into the energy transfer and charge transfer process. As shown in Fig. S6a,† the neat ITIC 珡lm shows a strong PL emission peak at 755 nm while the neat IT-4F 珡lm presents a relatively weak PL emission peak at 780 nm. A沢er blending IT-4F with ITIC, the blend 珡lm exhibits only one emission peak at 780 nm, which is identical with that of IT-4F. The characteristic peak of ITIC completely disappeared while the emission intensity of the ternary blend 珡lm increased remarkably. Since

Table 2 The electron and hole mobilities of binary and ternary blend films

Active layers	μ_e [cm^2 V^{-1} s^{-1}]	μ_h [cm^2 V^{-1} s^{-1}]	μ_e/μ_h
PBTA-PS:ITIC	1.85 × 10^{-4}	2.86 × 10^{-4}	0.64
PBTA-PS:IT-4F	3.42 × 10^{-4}	6.76 × 10^{-5}	5.05
Ternary blend	4.24 × 10^{-4}	3.86 × 10^{-4}	1.09

the absorption spectrum of IT-4F obviously overlaps with the PL emission spectrum, it can be concluded that efficient energy transfer from ITIC to IT-4F exists in the ternary system. Therefore, another possible channel to generate charges of ITIC excitons can be formed *via* such an energy transfer to IT-4F. The PL quenching in the blend 膜lms was also investigated. As displayed in Fig. S6b,† the neat PBTA-PS 膜lm exhibits an intense PL emission in the spectrum and it could be effectively quenched in both PBTA-PS:ITIC and PBTA-PS:IT-4F 膜lms, demonstrating an effective exciton dissociation between PBTA-PS and acceptors. A泪er adding IT-4F into the PBTA-PS:ITIC blend, the PL emission was further quenched, which is because of the effec- tive exciton dissociation between PBTA-PS and acceptors combined with an efficient energy transfer from ITIC to IT- 4F.[14,25] To further investigate the charge transport in the ternary system, the J_{SC} values of acceptor-only organic solar cells (OSCs) were measured and the corresponding J–V curves are shown in Fig. S7.† The J_{SC} values of OSCs based on ITIC and IT-4F neat
膜lms are 0.11 and 0.15 mA cm^{-2}, respectively. The ITIC:IT-4F device showed a J_{SC} of 0.21 mA cm^{-2}, which is comparable to that of the devices based on neat acceptors, revealing negligible transfer between ITIC and IT-4F. As a consequence, a泪er the exciton dissociation, the electrons could transport to ITIC and IT-4F individually and then be collected by the electrodes. Besides, the energy transfer from ITIC to IT-4F could help to enhance the exciton harvesting and dissociation between PBTA-PS and IT-4F. The superior exciton dissociation in the ternary system could guarantee high FF and PCE.

The surface and bulk morphology of binary and ternary blend 膜lms were characterized by atomic force microscopy (AFM) and transmission electron microscopy (TEM). As shown in Fig. 4a and b, both PBTA-PS:ITIC and PBTA-PS:IT-4F blend 膜lms exhibit smooth surfaces, with a root-mean-square (RMS) roughness of 1.77 and 1.12 nm, respectively. When 20% IT-4F was incorporated, the ternary blend 膜lms still exhibit a uniform surface with a moderate RMS roughness of 1.20 nm (Fig. 4c), which is between that of the PBTA-PS:ITIC and PBTA-PS:IT-4F binary 膜lms. Large grains are not observed, demon- strating a uniform nanoscale morphology. Meanwhile, as shown in TEM images, a泪er incorporating IT-4F, the ternary

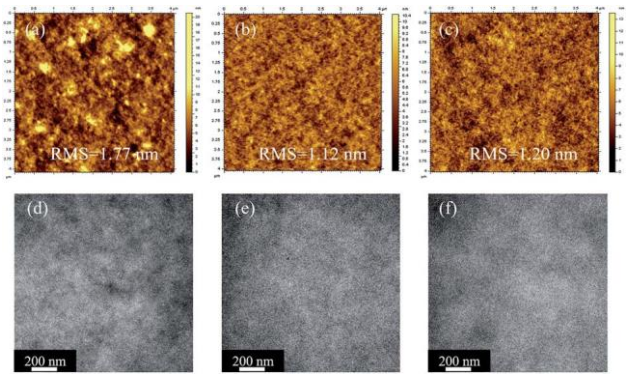

Fig. 4 AFM images of (a) PBTA-PS:ITIC, (b) PBTA-PS:IT-4F and (c) ternary blend films and TEM images of (d) PBTA-PS:ITIC, (e) PBTA-PS:IT-4F and (f) ternary blend films.

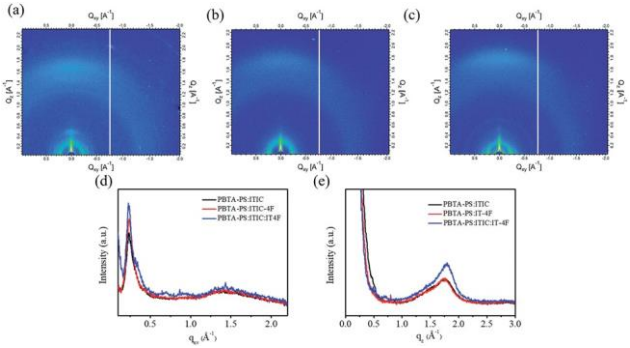

Fig. 5 2D-GIWAXS patterns for (a) PBTA-PS:ITIC, (b) PBTA:IT-4F and (c) ternary blend films. (d) In-plane and (e) out of plane line cuts of the corresponding 2D-GIWAXS pattern.

blend 膜lm exhibits a homogeneous morphology and no large phase separation was observed (Fig. 4d–f). This should be attributed to the good miscibility of the two acceptors. The appropriate morphologies are bene膜cial for exciton dissociation and charge transport, leading to high J_{SC} and FF.

Differential scanning calorimetry (DSC) measurement is conducted to further investigate the miscibility of acceptors in the blend 膜lm. As shown in Fig. S8,† there is no obvious thermal transition in the neat ITIC, IT-4F and their blend 膜lm, indicating that the miscibility of ITIC and IT-4F should be appropriate for constructing ternary blend PSCs.

The molecular packing and orientation of binary and ternary blend 膜lms are characterized by two-dimensional grazing-incidence wide-angle scattering (2D GIWAXS) measurement. The 2D GIWAXS patterns and the corresponding in-plane (IP) and out-of-plane (OOP) line cut pro膜les are shown in Fig. 5. The (100) lamellar diffraction peaks of PBTA-PS were observed for the binary and ternary blend 膜lms along the IP direction. Besides, PBTA-PS also exhibits (010) p–p stacking diffraction peaks along the OOP direction, indicative of preferential face-on orientation for PBTA-PS in the binary and ternary blend 膜lms. It is noteworthy that the ternary 膜lm shows obviously enhanced (100) and (010) peaks of PBTA-PS compared to binary 膜lms, indicative of a more ordered molecular packing of PBTA-PS in the ternary 膜lm. This might pro膜t the vertical charge transport and mitigation of carrier recombination, thus accounting for the high FF obtained in the ternary device. All these results prove that incorporating IT-4F into PBTA-PS:ITIC will not devastate the original molecular packing and orientation in the PBTA-PS:ITIC 膜lm. More importantly, IT-4F could work as a crystalline modulator, making the stacking of PBTA-PS more compact and more uniform in the ternary system.[46]

Conclusions

A series of high efficiency PSCs were fabricated by using PBTA-PS as the donor and two small molecules, ITIC and IT-4F, as acceptors. The ITIC and IT-4F based binary devices delivered PCEs of 11.83% and 9.55%, respectively. A泪er incorporating IT-4F into the PBTA-PS:ITIC system, the optimal ternary PSCs

delivered superior PCEs of 13.27% with a high J_{SC} of 19.60 mA cm^{-2} and an outstanding FF of 74.45%. The improved overall performance could be attributed to the good compatibility of the acceptors, enhanced light harvesting, more compact molecular stacking, more balanced charge transport and the efficient energy transfer between acceptors in the ternary blend 珐lms. Our result demonstrates that using a structurally similar acceptor as a crystalline modulator is a promising approach to enhance the molecular packing and realize highly efficient ternary PSCs.

Conflicts of interest

There are no con珍icts to declare.

Acknowledgements

The authors thank the National Natural Science Foundation of China (51773220, 51573205 and 61405209), the Shandong Provincial Natural Science Foundation (ZR2017ZB0314), DICP & QIBEBT (DICP&QIBEBT UN201709), and Dalian National Laboratory for Clean Energy (DNL) CAS for the 珐nancial support.

Notes and references

1 Y. Xie, W. Huang, Q. Liang, J. Zhu, Z. Cong, F. Lin, S. Yi, G. Luo, T. Yang, S. Liu, Z. He, Y. Liang, X. Zhan, C. Gao, H. Wu and Y. Cao, *ACS Energy Lett.*, 2018, 8–16, DOI: 10.1021/acsenergylett.8b01824.
2 X. Song, N. Gasparini, L. Ye, H. Yao, J. Hou, H. Ade and D. Baran, *ACS Energy Lett.*, 2018, 3, 669–676.
3 J. Y. Kim, K. Lee, N. E. Coates, D. Moses, T.-Q. Nguyen, M. Dante and A. J. Heeger, *Science*, 2007, 317, 222–225.
4 W. Chen, G. Huang, X. Li, H. Wang, Y. Li, H. Jiang, N. Zheng and R. Yang, *ACS Appl. Mater. Interfaces*, 2018, 10, 42747–42755.
5 T. M. Clarke and J. R. Durrant, *Chem. Rev.*, 2010, 110, 6736–6767.
6 Y. Liu, J. Zhao, Z. Li, C. Mu, W. Ma, H. Hu, K. Jiang, H. Lin, H. Ade and H. Yan, *Nat. Commun.*, 2014, 5, 5293.
7 W. Zhao, S. Li, H. Yao, S. Zhang, Y. Zhang, B. Yang and J. Hou, *J. Am. Chem. Soc.*, 2017, 139, 7148–7151.
8 J. Hou, O. Inganäs, R. H. Friend and F. Gao, *Nat. Mater.*, 2018, 17, 119.
9 L. Dou, Y. Liu, Z. Hong, G. Li and Y. Yang, *Chem. Rev.*, 2015, 115, 12633–12665.
10 S. Li, L. Ye, W. Zhao, S. Zhang, S. Mukherjee, H. Ade and J. Hou, *Adv. Mater.*, 2016, 28, 9423–9429.
11 Z. Fei, F. D. Eisner, X. Jiao, M. Azzouzi, J. A. Röhr, Y. Han, M. Shahid, A. S. R. Chesman, C. D. Easton, C. R. McNeill, T. D. Anthopoulos, J. Nelson and M. Heeney, *Adv. Mater.*, 2018, 30, 1705209.
12 W. Zhao, S. Zhang, Y. Zhang, S. Li, X. Liu, C. He, Z. Zheng and J. Hou, *Adv. Mater.*, 2017, 30, 1704837.
13 X. Xu, T. Yu, Z. Bi, W. Ma, Y. Li and Q. Peng, *Adv. Mater.*, 2017, 30, 1703973.
14 W. Chen, H. Jiang, G. Huang, J. Zhang, M. Cai, X. Wan and R. Yang, *Sol. RRL*, 2018, 2, 1800101.
15 Y. Zhang, B. Kan, Y. Sun, Y. Wang, R. Xia, X. Ke, Y.-Q.-Q. Yi, C. Li, H.-L. Yip, X. Wan, Y. Cao and Y. Chen, *Adv. Mater.*, 2018, 30, 1707508.
16 X. Che, Y. Li, Y. Qu and S. R. Forrest, *Nat. Energy*, 2018, 3, 422–427.
17 J. Yan, Q. Liang, K. Liu, J. Miao, H. Chen, S. Liu, Z. He, H. Wu, J. Wang and Y. Cao, *ACS Energy Lett.*, 2017, 2, 14–21.
18 W. Chen, M. Xiao, L. Han, J. Zhang, H. Jiang, C. Gu, W. Shen and R. Yang, *ACS Appl. Mater. Interfaces*, 2016, 8, 19665–19671.
19 T. Ameri, P. Khoram, J. Min and C. J. Brabec, *Adv. Mater.*, 2013, 25, 4245–4266.
20 W. Shen, W. Chen, D. Zhu, J. Zhang, X. Xu, H. Jiang, T. Wang, E. Wang and R. Yang, *J. Mater. Chem. A*, 2017, 5, 12400–12406.
21 L. Lu, M. A. Kelly, W. You and L. Yu, *Nat. Photonics*, 2015, 9, 491.
22 R. Lv, D. Chen, X. Liao, L. Chen and Y. Chen, *Adv. Funct. Mater.*, 2019, 1805872.
23 N. Gasparini, X. Jiao, T. Heumueller, D. Baran, G. J. Matt, S. Fladischer, E. Spiecker, H. Ade, C. J. Brabec and T. Ameri, *Nat. Energy*, 2016, 1, 16118.
24 R. Yu, H. Yao and J. Hou, *Adv. Energy Mater.*, 2018, 8, 1702814.
25 Q. An, F. Zhang, J. Zhang, W. Tang, Z. Deng and B. Hu, *Energy Environ. Sci.*, 2016, 9, 281–322.
26 Z. Li, X. Xu, W. Zhang, X. Meng, Z. Genene, W. Ma, W. Mammo, A. Yartsev, M. R. Andersson, R. A. J. Janssen and E. Wang, *Energy Environ. Sci.*, 2017, 10, 2212–2221.
27 T. Ameri, P. Khoram, T. Heumüller, D. Baran, F. Machui, A. Troeger, V. Sgobba, D. M. Guldi, M. Halik, S. Rathgeber, U. Scherf and C. J. Brabec, *J. Mater. Chem. A*, 2014, 2, 19461–19472.
28 N. Felekidis, E. Wang and M. Kemerink, *Energy Environ. Sci.*, 2016, 9, 257–266.
29 P. Yin, T. Zheng, Y. Wu, G. Liu, Z.-G. Zhang, C. Cui, Y. Li and P. Shen, *J. Mater. Chem. A*, 2018, 6, 20313–20326.
30 Y. Xie, F. Yang, Y. Li, M. A. Uddin, P. Bi, B. Fan, Y. Cai, X. Hao, H. Y. Woo, W. Li, F. Liu and Y. Sun, *Adv. Mater.*, 2018, 30, 1803045.
31 Z. Zhou, S. Xu, J. Song, Y. Jin, Q. Yue, Y. Qian, F. Liu, F. Zhang and X. Zhu, *Nat. Energy*, 2018, 3, 952–959.
32 T. Liu, Y. Guo, Y. Yi, L. Huo, X. Xue, X. Sun, H. Fu, W. Xiong, D. Meng, Z. Wang, F. Liu, T. P. Russell and Y. Sun, *Adv. Mater.*, 2016, 28, 10008–10015.
33 R. Yu, S. Zhang, H. Yao, B. Guo, S. Li, H. Zhang, M. Zhang and J. Hou, *Adv. Mater.*, 2017, 29, 1700437.
34 B. Kan, Y.-Q.-Q. Yi, X. Wan, H. Feng, X. Ke, Y. Wang, C. Li and Y. Chen, *Adv. Energy Mater.*, 2018, 8, 1800424.
35 X. Ma, W. Gao, J. Yu, Q. An, M. Zhang, Z. Hu, J. Wang, W. Tang, C. Yang and F. Zhang, *Energy Environ. Sci.*, 2018, 11, 2134–2141.
36 M. Zhang, Z. Xiao, W. Gao, Q. Liu, K. Jin, W. Wang, Y. Mi, Q. An, X. Ma, X. Liu, C. Yang, L. Ding and F. Zhang, *Adv. Energy Mater.*, 2018, 1801968.

37 W. Huang, P. Cheng, Y. Yang, G. Li and Y. Yang, *Adv. Mater.*, 2018, **30**, 1705706.
38 L. Nian, Y. Kan, H. Wang, K. Gao, B. Xu, Q. Rong, R. Wang, J. Wang, F. Liu, J. Chen, G. Zhou, T. P. Russell and A. K. Y. Jen, *Energy Environ. Sci.*, 2018, **11**, 3392–3399.
39 W. Zhao, S. Li, S. Zhang, X. Liu and J. Hou, *Adv. Mater.*, 2016, **29**, 1604059.
40 J. Zhang, Y. Zhang, J. Fang, K. Lu, Z. Wang, W. Ma and Z. Wei, *J. Am. Chem. Soc.*, 2015, **137**, 8176–8183.
41 M. Lenes, M. Morana, C. J. Brabec and P. W. M. Blom, *Adv. Funct. Mater.*, 2009, **19**, 1106–1111.
42 Q. An, W. Gao, F. Zhang, J. Wang, M. Zhang, K. Wu, X. Ma, Z. Hu, C. Jiao and C. Yang, *J. Mater. Chem. A*, 2018, **6**, 2468–2475.
43 P. Yin, T. Zheng, Y. Wu, G. Liu, Z.-G. Zhang, C. Cui, Y. Li and P. Shen, *J. Mater. Chem. A*, 2018, **6**, 20313–20326.
44 Q. Liang, J. Han, C. Song, X. Yu, D.-M. Smilgies, K. Zhao, J. Liu and Y. Han, *J. Mater. Chem. A*, 2018, **6**, 15610–15620.
45 J. Yuan, Y. Xu, G. Shi, X. Ling, L. Ying, F. Huang, T. H. Lee, H. Y. Woo, J. Y. Kim, Y. Cao and W. Ma, *J. Mater. Chem. A*, 2018, **6**, 10421–10432.
46 B. Fan, X. Du, F. Liu, W. Zhong, L. Ying, R. Xie, X. Tang, K. An, J. Xin, N. Li, W. Ma, C. J. Brabec, F. Huang and Y. Cao, *Nat. Energy*, 2018, **3**, 1051–1058.